Available online at www.uofk.edu/uofkej

UofKEJ Vol. 4 Issue 2 pp. 48-57 (February 2014)

UNIVERSITY OF KHARTOUM ENGINEERING JOURNAL (UOFKEJ)

Pixel-Vernier: A General Image-Based Approach For Particle Size Distribution Estimation

Gamal H. Seedahmed[1] and Andy L. Ward[2]

[1]*Department of Surveying Engineering, Faculty of Engineering, University of Khartoum Khartoum, Sudan (E-mail: Gamal.Seedahmed@gmail.com)*

[2]*Caribbean Institute for Meteorology and Hydrology, Bridgetown, Barbados (E-mail: award@cimh.edu.bb)*

Abstract Particle size distribution estimation (PSDE) is a fundamental task for heterogeneous materials characterization and modeling. This paper presents a general image-based approach for PSDE, which is called collectively “Pixel-Vernier” or PV for short. Meaningful image segmentation is the main problem to be solved for image-based PSDE. To this end, the proposed approach combines markers-controlled watershed segmentation with a clustering algorithm to solve the delineation of the boundaries of the particles. The combined approach is embedded in a coarse-to-fine strategy using a one training parameter to adapt the algorithm to the underlying distributions of the particle size. This training parameter is restricted to the size of an averaging filter. PV decomposes the image into separate particle regions. The final results of these regions are used to compute several geometric attributes for particles such as the semi-major axis, the semi-minor axis, and the equivalent diameter. Then, the geometric attributes of all the particles are used to estimate size distribution and relevant statistics. PV can be used in a laboratory as well as in a field setting. It is tested successfully on a diverse set of images that represent materials like soils, texture, rocks, and Mars surface geology.

Keywords: *Image segmentation; Smoothing; Clustering; Particle size; Distribution estimation.*

1. INTRODUCTION

Particle size distribution estimation (PSDE) is a fundamental task for materials understanding, characterization, and modeling. Although the major focus of this paper is on soil particles size estimation and characterization, the presented work can be adapted to a wide spectrum of applications such as chemical products and process engineering [1]. For example, by estimation and control of the particle size distribution, we can control and predict the product and process characteristics. In the last two decades, image-based PSDE emerges as a strong research direction complementing the existing methods and overcoming some of their limitations. As a major observation, the progress in image-based PSDE research is strongly linked to two contradicting factors. First, the scientific development and advancement in several interrelated computational fields, such as digital image processing, computer vision, and digital photogrammetry. Second, the development and advancement made slowly penetrate the PSDE. These two factors are well reflected in the early and the recent approaches for PSDE. For example, in the eighties and early nineties photo-sieving [2] and [3] is proposed as a method for image-based PSDE. Photo-sieving relies on manual identification and digitization of individual particle boundaries. On the other hand, Butler *et al*., [4] utilized a simple global threshold approach for particles delineation or segmentation assuming that the image intensities follow a bimodal distribution. They tested an automated approach for threshold selection and they found that it has a very poor performance and so the threshold was selected subjectively. It is clear that in general, image-based segmentation or partitioning that depends only on thresholding do not produce acceptable results in the gamut of image segmentation applications; and this is due to the complexity associated with the image formation process.

A gradual progress was made toward developing more sophisticated approaches for PSDE. For example, Ghalib and Hryciw [5] presented a comprehensive approach for soil PSDE using digital images acquired in a laboratory setting. They used a backlight illumination to enhance the contrast of the particles. Their approach starts with a binary thresholding and then was followed by distance transform and watershed segmentation for the final delineation of the particle regions. McEwan *et al.* [6] used Canny edge detection followed by morphological dilation and skeletonization to delineate sediment particles imaged by a high-resolution laser altimeter. Researchers argued that this approach can be extended to digital images with additional development. In another laboratory setting, Carter and Yan

[7] investigated the suitability of image-based particle size analyzer for measuring particle shape parameters, such as aspect ratio. They concluded that the imaging-based sensor is very capable of measuring shape parameters within acceptable tolerance bounds.

Graham *et al*. [8] offered a detailed analysis of four approaches for automated particle size measurement of coarse-grained sediments that exceed 23μm. All of the parameters that control the performance of these approaches were tested for every possible combination to identify the range of values that will give acceptable results. From a computational learning perspective, their testing methodology is equivalent to partial ensemble methods or classifier combinations [9]. One of the tested approaches in Graham *et al*. [10] will be reviewed in more details in the next paragraph because it is relevant in some aspects to the presented paper.

Graham *et al.* [10] developed a sophisticated image-based approach for PSDE. Their approach followed a coarse-to-fine or a global-to-local strategy for particles or grains extraction. This approach starts with a non-linear smoothing by a median filter to remove the markings from the particle surfaces while preserving the edges. This step is followed by a morphological bottom-hat transform to identify small dark parts of an image. Then a double threshold approach is applied to the transformed image to obtain an initial segmentation. Then his result is refined by a watershed segmentation that is augmented by minima suppression. The overall performance of the algorithm is optimized by a detailed assessment of its internal parameters, which are tuned to work with image particles that are bigger than 23μm. The final results should be checked visually in case the segmentation step has failed for some reason. The approach adopted in this paper is different in two major aspects: (1) it is very general and can be trained to accommodate any particle size distribution; (2) it addresses the complexity of the segmentation problem in an integrated and robust way. This approach follows gradual steps to identify the hypotheses for the image regions that correspond to particles.

From the previous discussion, it is evident that the core of an image-based PSDE is highly dependable on a robust segmentation procedure to isolate the particles regions from their backgrounds. Practically, the success of any image segmentation algorithm is typically judged by the extent to which acceptable results can be obtained and the computational efficiency with which these results can be delivered. To this end, the paper presents a general approach for image-based PSDE using an integrated and a multi-stage segmentation approach. As stated, the proposed approach is called collectively “Pixel-Vernier” or (PV) for short. PV combines markers-controlled watershed segmentation, which will be explained in the next section, and a minimum-distance clustering and thresholding algorithm for particle regions extraction. PV is embedded in coarse-to-fine strategy to perform the extraction process of particles regions. From a computational learning perspective, PV works in a supervised mode of learning that requires a training sample or information. In this work, training information is restricted to a single smoothing parameter to adapt PV to the underlying size of the targeted particle distribution. The extracted regions are used to derive several geometric attributes for each particle, such as the semi-major axis, the semi-minor axis, and the equivalent diameter. Then, these geometric attributes of all particle regions are used to estimate the particle size distribution and their relevant statistics. PV can be used in a laboratory as well as a field setting. PV is tested successfully in a diverse set of materials such as soils, texture, rocks, and Mars surface images.

This paper is organized as follows. Section two outlines the details of the proposed approach. Section three provides the experimental results and their discussions; and finally, section four concludes the paper.

2. PROPOSED APPROACH

Pixel-Vernier (PV) is a supervised learning approach for image-based particle size distribution estimation (PSDE) that uses a single training parameter. In addition, PV can be viewed as a measurement approach for particles distribution estimation that exploits human cognition and abstraction of decision-making at a relatively high level. The training parameter of PV is confined to the size of an averaging filter. The user will check the result visually at the training stage to determine if the results are acceptable or not in terms of delineating the optimal image regions that correspond to the particles in question. The benefits of the averaging process can be appreciated from several angles such as minimizing the local random variability, increasing the probability of getting connected component for the particle regions, removing markings on the particle surfaces, and introducing the bias of the PV user/s toward a particular size distribution. From the classical setting of non-linear problems solving, the training step or the smoothing process can be perceived as provision of initial approximation for the segmentation algorithm to converge to a particular size. This approximation does not have to be exact, but it has a wide radius of convergence. From this perspective, the zero approximation should be considered as one of the options. In other words, some applications may not require any approximations and the algorithm will converge to the correct size without smoothing. Most likely this is the case for highly textured images such as fine grained soil. After obtaining the optimal averaging window size by training, PV proceeds in two phases of segmentations to extract the particle regions following a coarse-to-fine strategy. At the coarse level, we developed markers-controlled watershed segmentation algorithm, which is also a two-stage process. In other words, the first stage is a collective action of preprocessing by markers and then followed in the second stage by the classical watershed segmentation. Markers are generally defined as local connected image regions that can be grouped based on homogeneity or other criteria of similarity [11]. The markers limit the number of image regions that will result from the watershed segmentation. At the fine level or the second stage, PV uses a minimum distance clustering algorithm for local segmentation within every region that results from the coarse

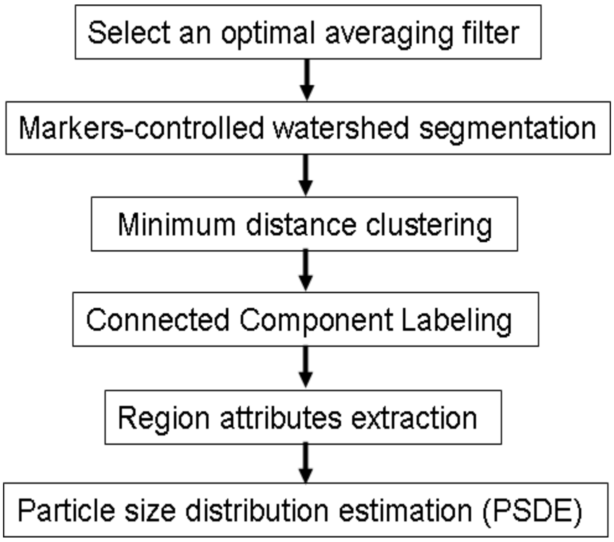

Fig. 1. The overall work flow of proposed approach

level segmentation. The minimum distance clustering was developed to offset the remaining local over-segmentation induced by watershed algorithm. The final results of the of the minimum distance clustering, in terms of the final segmented image regions, is forwarded to a connected component labeling algorithm Shapiro and Stockman, [12] to identify and to extract each image region. Fig. 1 shows the overall work flow of the proposed approach. In the following subsections we will give a detailed discussion of the elements of the proposed approach.

2.1 Markers-Controlled Watershed Segmentation

Markers-controlled watershed segmentation is a powerful approach for image segmentation [13]. This approach allows development of practical solutions to the over-segmentation problem associated with the classical watershed algorithm by limiting the number of image regions. This limitation is typically achieved by adding a preprocessing step (here: markers) that can bring extra knowledge into the watershed segmentation algorithm [11]. As a side remark, from a cognitive science perspective, markers can be viewed as a mechanism that brings a focus of attention to selected areas in the image. Itti and Koch [14] defined attention as the process of selecting and gating visual information based on saliency in the image itself (bottom-up), and on prior knowledge about scenes, objects, and their interrelations (top-down). Practically, a marker is a local homogenous connected component (a region) that belongs to an image. By viewing the information content of an image as a foreground and a background, two types of markers could be defined. Internal and external markers, which belong to the foreground and the background, respectively. Different types of image attributes can be used as markers such as intensity, color, edge gradients, texture, and even motion in the case of an image sequence. In general, a procedure for marker selection has two main steps: (1) Identification of the image attributes that will be used to define the marker; and (2) Implementation of the preprocessing.

In the context of the proposed approach in this paper, the marker control is achieved through the use of a set of ranking filters to enhance the information content of the image. The image intensities in a predefined local neighborhood are sorted according to their numerical values and then the central pixel in that neighborhood is replaced by a ranked intensity value selected according to a preset criterion such as the minimum or the maximum [15]. In particular, markers control step is applied as follows:

a. A circular local neighborhood, which has a radius of 5 pixels, is chosen for the ranked filters. The circular shape is chosen to minimize the directional effects of the local neighborhood.
b. Two new images are generated by convolving the original image by the maximum and the minimum rank filters. We call them the maximum image and the minimum image, respectively. In fact, the maximum filter is nothing compared to the classical top hat filter [16].
c. The maximum image is added to the original image to form a new image. The objective of this step is to enhance the local boundaries.
d. The minimum image obtained in step (b) is subtracted from the end result of step (c) to produce a new image.
e. A complement image is computed for the new image obtained in step (d). To understand the notion of the complement image, let us consider the following two examples. In the complement of a binary image, zeros become ones and ones become zeros. In other words, black and white are reversed. In the complement of intensity or gray level image, each pixel value is subtracted from the maximum pixel value (e.g., 255) supported by the class. The difference is used as the pixel value in the output image. In the output image, dark areas become lighter and light areas become darker.
f. The complement image is forwarded to the classical watershed segmentation algorithm to obtain an initial hypothesis for the particle regions.

2.2 Minimum Distance Clustering Algorithm

Although the combined approach of the markers-controlled and the smoothing process offer a solution to the global over-segmentation problem encountered in the watershed algorithm, it led to a local over-segmentation at the level of a particle region. In other words, the image regions do not provide optimal information for the existing particles in terms of their spatial extent. To solve this, we developed a minimum distance clustering algorithm to handle the local over-segmentation. The underlying principle of this algorithm is based on the assumption that of separable intensity distribution within each image region into two classes, which is the classical objective of any binary thresholding approach. As a side remark, the result of any binary thresholding depends on how the thresholding value or the decision-line is selected or obtained. For example, manual selection of the threshold reflects the human bias towards a particular intensity distribution. On the other hand, automatic selection of the threshold value typically reflects a certain statistical tendency. For example, Otsu's algorithm [17] seeks the bimodal distribution between two classes by minimizing the within-group variance and maximizing the between-group variance. The minimum distance clustering algorithm is based on the following:

a. Searching for the minimum and maximum intensity values within each image region that resulted from the markers-controlled watershed segmentation.
b. Classifying the intensity values in each region into two classes according to their absolute distance from the minimum and the maximum intensity values in each particular region.
c. The pixels with intensity values that are close to the maximum intensity are classified as particles and the ones that are close to the minimum are classified as backgrounds. This classification assumes that the particle intensities have a bias toward the brightest or highest intensity values, but nothing wrong with taking the opposite bias, which will become application dependent.

Fig. 2 shows the conceptual diagram for the minimum distance clustering algorithm. The oval on the top resembles a mixed intensity distribution, but after applying the minimum distance clustering algorithm is separated into two classes as shown by the left and right ovals on the bottom.

2.3 Geometric Attributes Extraction

Following Shapiro and Stockman [12], the following region properties were derived from the results of the combined approach:

a. Region area, which is the number of pixels per each region.
b. Region boundaries.
c. Perimeter length (P), which are the number of the pixels along the boundary of a region. The perimeter length is used to derive what is called the 'equivalent diameter (ED)' as follows:

$$\mathrm{ED} = \frac{\mathrm{P}}{\pi} \quad (1)$$

d. Region centroid combined with its boundary to derive three types of moments. These moments are the second-order row moment, the second-order column moment, and the second-order mixed moments. These moments were combined together to derive geometrical attributes of the best fit ellipse to each image region. The attributes are the length of the semi-major (a) and the semi-minor (b) axes. These two attributes were used to derive the average anisotropy of the all extracted particles (n) as follows:

$$\text{Anisotropy} = 1 - \frac{1}{n}\sum_{i=1}^{n}\frac{b_i}{a_i} \quad (2)$$

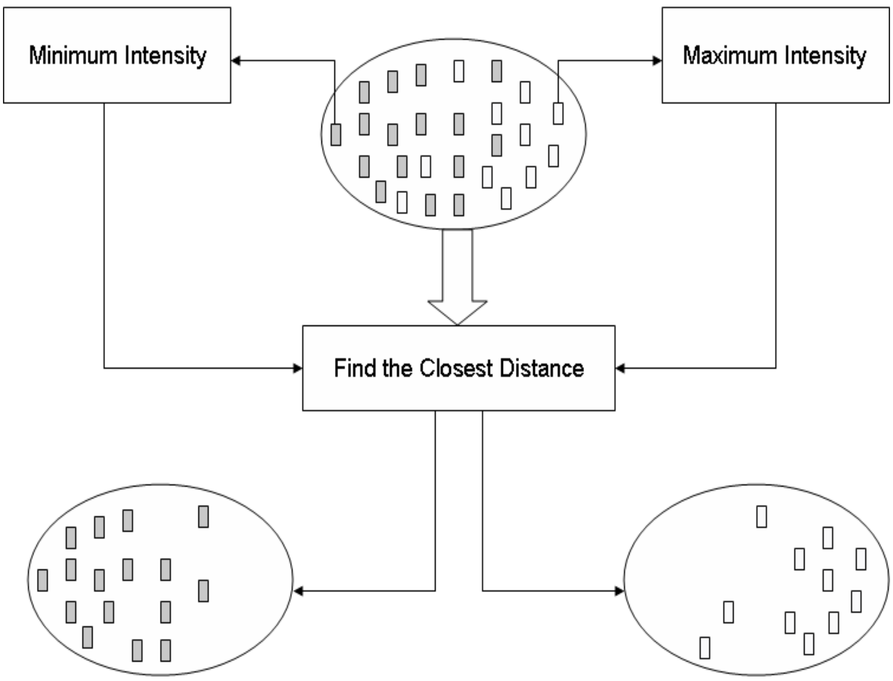

Fig. 2. A conceptual diagram for the minimum distance clustering algorithm

.

2.4 Particles-Size Distribution Estimation and Statistics

The equivalent diameters (EDs), or diameters for short, of the entire particles that exist within an image view were used to derive cumulative distribution curve, which was obtained from a histogram. The information content (frequency counting) of each bin in the histogram is weighted by the corresponding areas of the diameters that contribute to each bin. This weighting is used to account for the actual 2-D coverage of the image regions or particles. Naïve Frequency counting will lead to incorrect characterization of the particle size distribution estimation (PSDE). Mathematically, the frequency weighting of the equivalent diameter (ED) is implemented as follows:

$$\hat{f}(ED) = \sum_{i=1}^{m} A_i ED_i \qquad (3)$$

where $\hat{f}$ is the estimated frequency for the ED and A_i is the corresponding area for each ED. Following Folk (1980), the cumulative distribution curve is used to estimate the following statistical measures:

a. Median, this is the ED that corresponds to the 50% mark on the cumulative curve. Computationally the median is given by:

$$\text{Median} = ED_{50\%} \qquad (4)$$

b. Graphic mean (M_z) and is given by:

$$M_z = \frac{ED_{16\%} + ED_{50\%} + ED_{84\%}}{3} \qquad (5)$$

c. Inclusive graphic standard deviation, σ_I, is given by:

$$\sigma_I = \frac{ED_{84\%} - ED_{16\%}}{4} + \frac{ED_{95\%} - ED_{5\%}}{6.6} \qquad (6)$$

d. Inclusive Graphic skewness (SK_I) averages the skewness obtained from $ED_{16\%}$ and $ED_{84\%}$ with the skewness obtained from $ED_{5\%}$ and $ED_{95\%}$. This measure is given by:

$$SK_I = \frac{ED_{16\%} + ED_{84\%} - 2 \times ED_{50\%}}{2 \times (ED_{84\%} - ED_{16\%})} + \frac{ED_{5\%} + ED_{95\%} - 2 \times ED_{50\%}}{2 \times (ED_{95\%} - ED_{5\%})} \qquad (7)$$

SK_I determines the skewness of the central portion of the cumulative curve as well as the skewness of the "tails". The tails are just formed where the most critical differences between samples lie.

e. Graphic kurtosis, and is given by:

$$K_G = \frac{ED_{95\%} - ED_{5\%}}{2.44 \times (ED_{75\%} - ED_{25\%})} \qquad (8)$$

For normal curve, K_G=1.00; leptokurtic curves have K_G over 1.00; and platykurtic curves have K_G less than 1.00.

3. RESULTS AND DISCUSSION

A MATLAB(R) prototype software was developed to implement the proposed approach. A series of experiments will be reported to demonstrate the validity and the generality of the proposed approach (PV). The first set of experiments will be used to show the computational correctness of PV and its predictive capability of ground truth information in terms of known diameters. PV will be used to estimate the mean, median, inclusive graphic standard deviation, inclusive Graphic skewness, inclusive graphic kurtosis, and anisotropy for each image of the particle distribution. As stated previously, the correctness of the segmentation or the particle regions delineation results will be judged visually at the training stage. This training will be achieved by searching for an optimal window size of smoothing filter.

A Sony XC-555 microscopic digital video camera was used to acquire four images with known average distribution sizes; see **Fig. 3.** This camera is equipped with a fixed focal

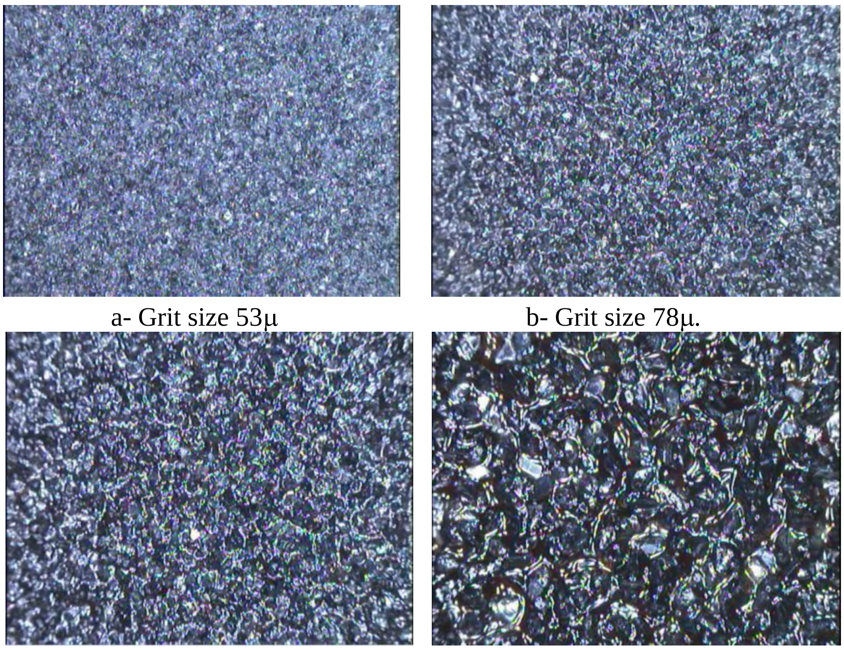

a- Grit size 53μ   b- Grit size 78μ.

c- Grit size 116μ   d- Grit size 278μ

Fig. 3. The Four images taken by Sony XC-555 microscopic digital video camera

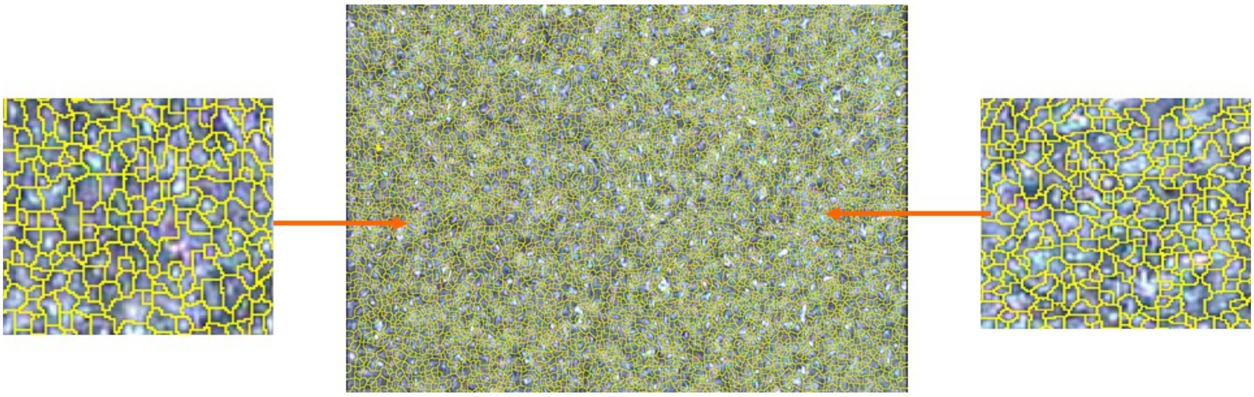

Fig. 4. Markers-controlled watershed segmentation for the image shown in Fig. 3.a.

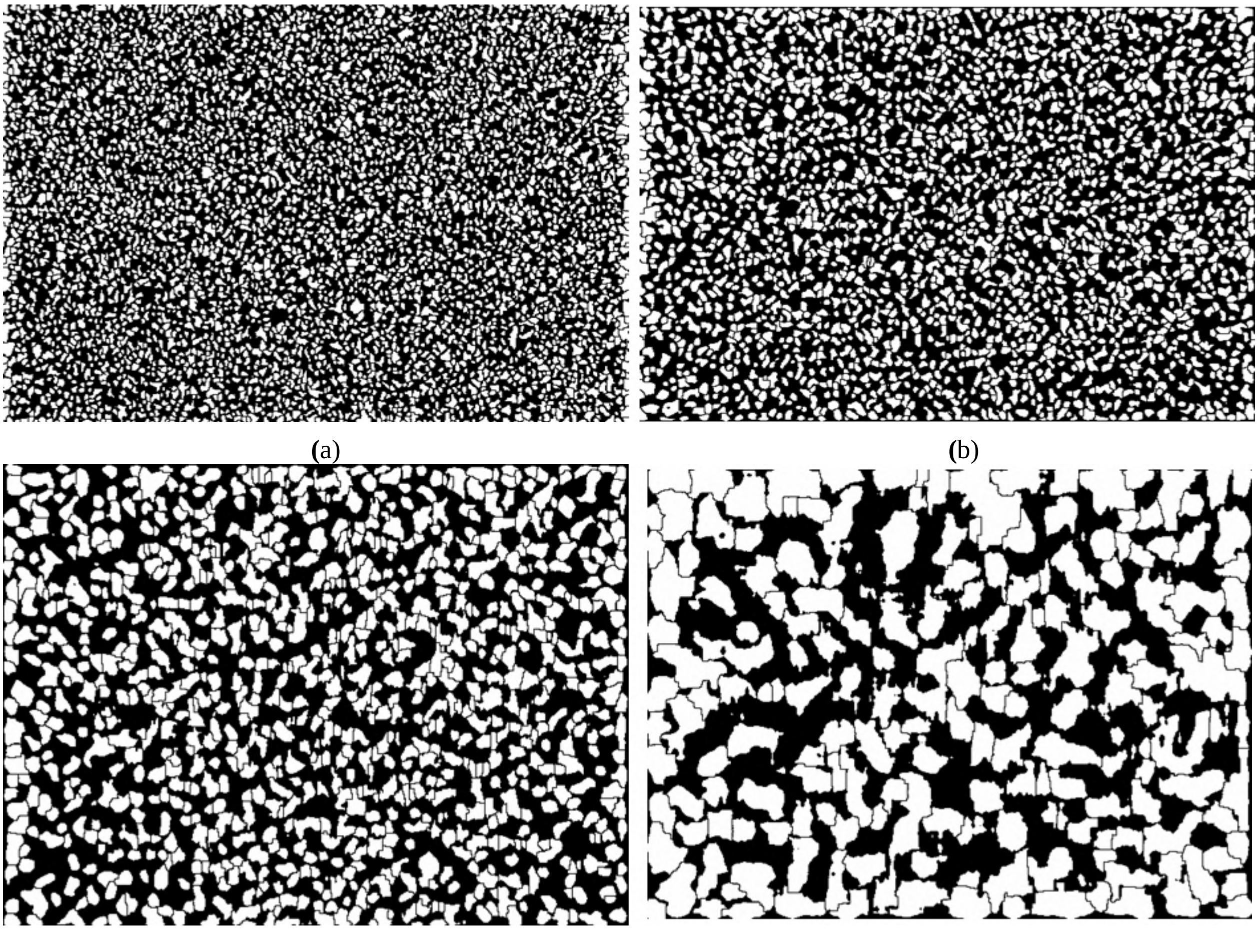

(a) (b) (c) (d)

Fig. 5. The final segmentation results for the images shown in Fig. 3

length, 6.4 mm, and it has an effective image size of 768 x 494 pixels. The average particle or grit sizes captured by each image are 53μ, 78μ, 116μ, and 278μ, respectively. The spatial resolution of the four images is 10μ/pixel. In other words, every pixel represents 10μ. **Fig. 4** shows the results of the markers-controlled watershed segmentation on the image depicted in **Fig. 3.a**. The yellow boundaries highlight the particle regions at the coarse level. The local over-segmentation is very clear in each region, as shown by the zoom-in patches appearing to the left and the right. This result justifies the use of the minimum distance clustering algorithm to refine or to delineate the optimal region. Fig. 5 shows the binary images for the results of the minimum distance clustering and the white regions refer to the delineated particles. **Fig. 6** shows the cumulative distributions for the diameters of the particle images displayed in **Fig. 5**. **Table 1** shows the estimated statistics for the particle distribution of the images shown in **Fig. 3**. The second column in Table 1 and the rest of the tables depict the actual average values for the particle associated with each image.

The results shown in **Table 1** suggest that PV reproduces the actual mean diameters for the four distributions with a very

Table 1. The estimated statistics for the images shown in Fig. 3.

Image ID	Actual Mean Diameter (μm)	Window Size (pixels)	Mean Diameter (μm)	Median (μm)	σ_I (μm)	SK_I	K_G	Anisotropy
a	53	3	53.032	53.635	16.406	-0.137	1.111	0.376
b	78	5	73.400	73.700	16.770	-0.055	0.836	0.354
c	116	7	113.360	115.63	31.868	0.162	0.929	0.360
d	278	17	277.960	270.190	68.652	0.14978	0.993	0.354

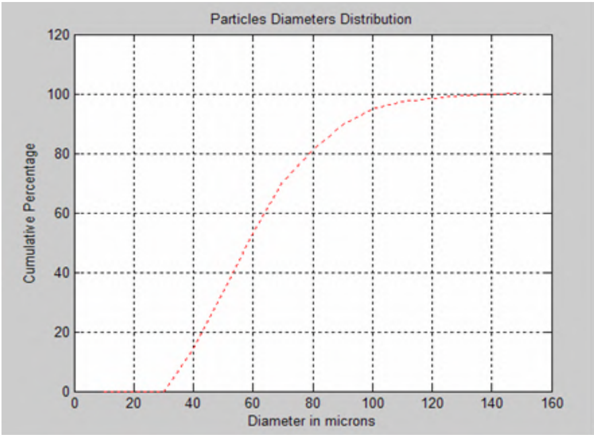

(a)

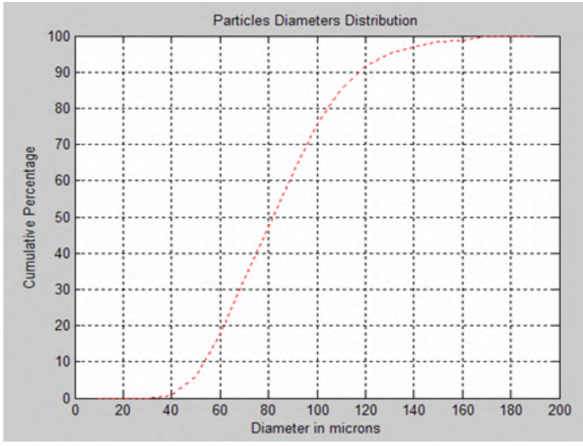

(b)

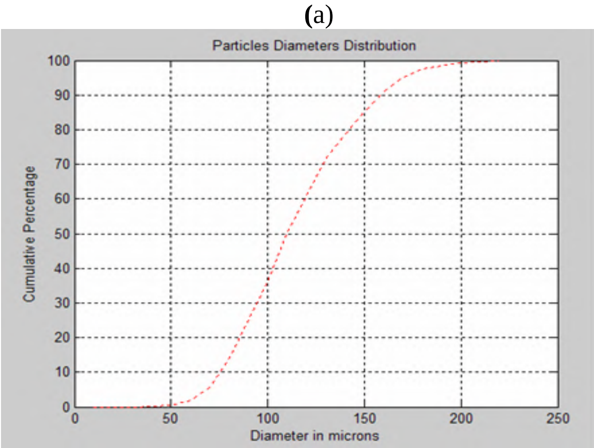

(c)

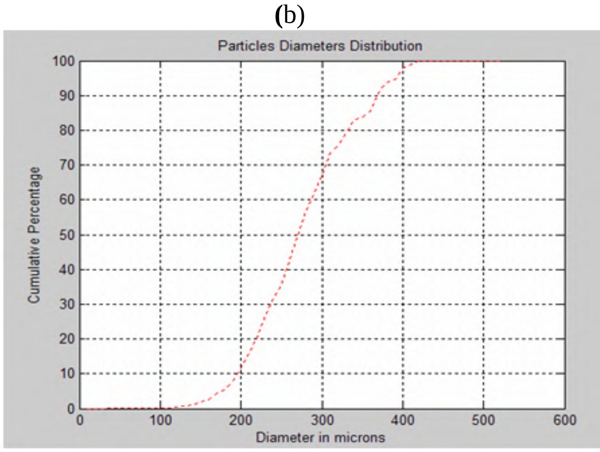

(d)

Fig. 6. The cumulative distribution of the diameters for the particles images shown in Fig. 5

small deviation in image b and c. The selection of the optimal window size for the averaging filter, as shown in **Table 1**, is very robust that is not being very close to the actual value of the diameter. For example, the window size for image number (c) is 17 pixels, which is equal to 170μm. This value is very far from the true value (278μm) shown in **Table 1**. It is very interesting to observe the closeness between the mean and the median, which is a strong indicator for the unbiasedness of mean values. In other words, the mean diameter is a representative measure for the whole distribution captured by the image. This is because closeness explains the fact that there are errors cancellation in the averaging process that produces the mean values since there are symmetrical distribution of the errors to the left and right of the mean values. More precisely, the probability of errors of commission and omission are equal. In the context of this work, commission and omission refer to over and under segmentation of the particles or image objects. Fundamentally, these errors are induced by the complexity of digital image formation process, which are not completely captured by the image segmentation algorithm. Thanks to the combined interplay between the mean and the median in delivering robust results despite the large values of standard deviation (see column in **Table 1**). The averaging does the errors cancellation and the median provides the information if there is symmetry or not. The last column of Table 1 shows anisotropy as computed by equation (2), which is a very hard measure to get by normal thieving. In addition, the deviation of anisotropy from zero clearly defeats any hypothesis for sphericity or isotropy.

The following experiment will be used to show the applicability of PV on general particle patterns with a

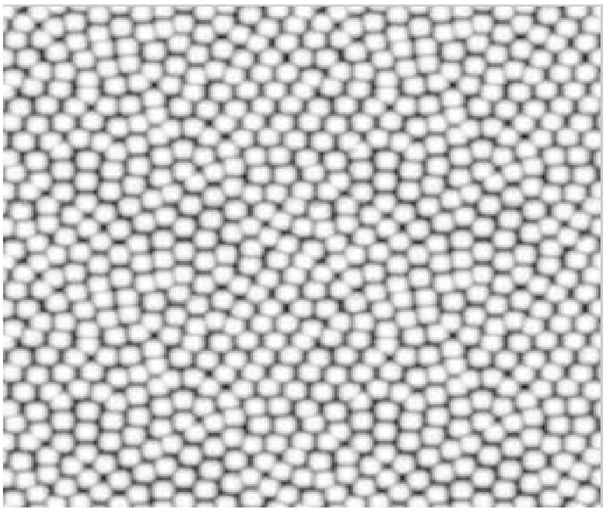

Fig. 7. A snake skin texture image

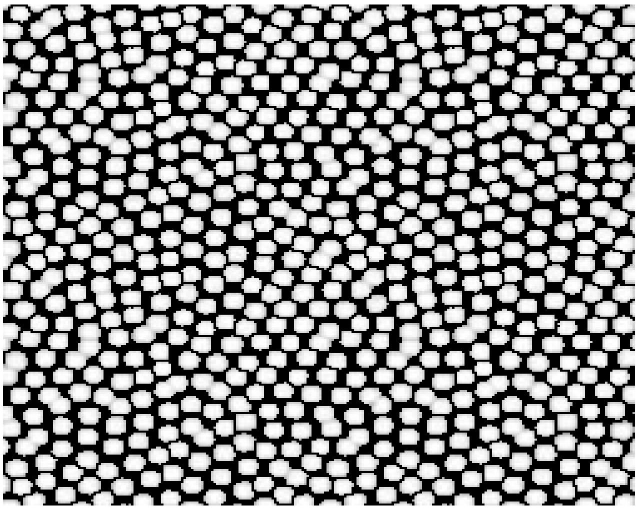

Fig. 8. Snake skin segmentation

Table 2. The estimated parameters for the snake skin image.

Image ID	Actual Mean Diameter (pixels)	Window Size (pixels)	Mean Diameter	Median (pixels)	σ_I (pixels)	SK_I	K_G	Anisotropy
Snake skin	9.5 ±1	5	10.731	8.101	0.490	-1.912	1.4381	0.251

Fig. 9. An image of rock particles

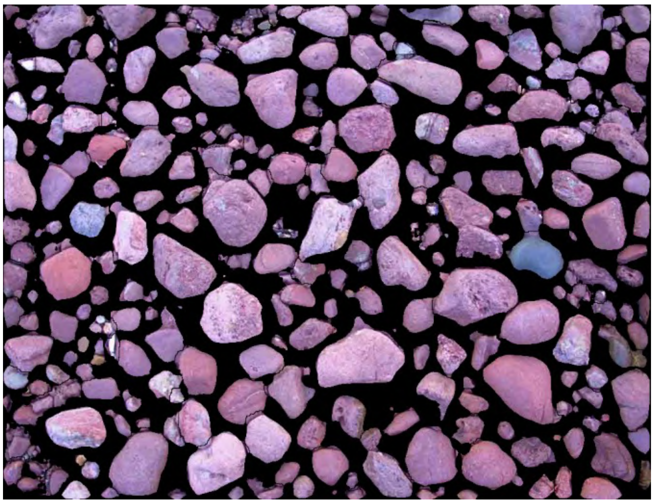

Fig. 10. Segmentation results of the rock particles image

Table 3. The estimated parameters for the rock particles image

Image ID	Window Size (pixels)	Mean Diameter (pixels)	Median (pixels)	σ_I (pixels)	SK_I	K_G	Anisotropy
Rock Particles	17	32.983	34.648	7.585	-0.268	0.925	0.323

manually obtained ground truth. **Fig. 7** shows a texture image of a snake skin. The manual measurement of the average diameter for the texture elements is 9.5 ±1 pixels. **Fig. 8** shows the final segmentation results and **Table 2** presents the relevant parameters estimated by PV.

From **Table 2** we can come to the following observations. First, the proposed algorithm (PV) provides a very close estimate for the average diameter (10.731 pixels) in light of its ground truth value (9.5 pixels). Second, although the algorithm resulted in incorrect segmentation in terms of

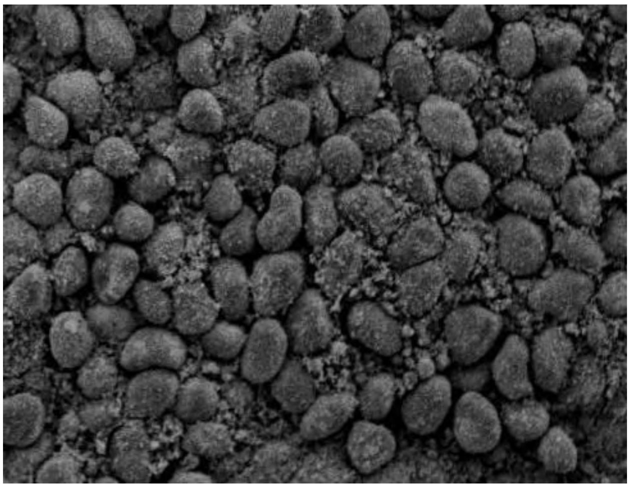

Fig. 11. An image of Mars surface.
(Image courtesy of NASA/JPL/Cornell/USGS)

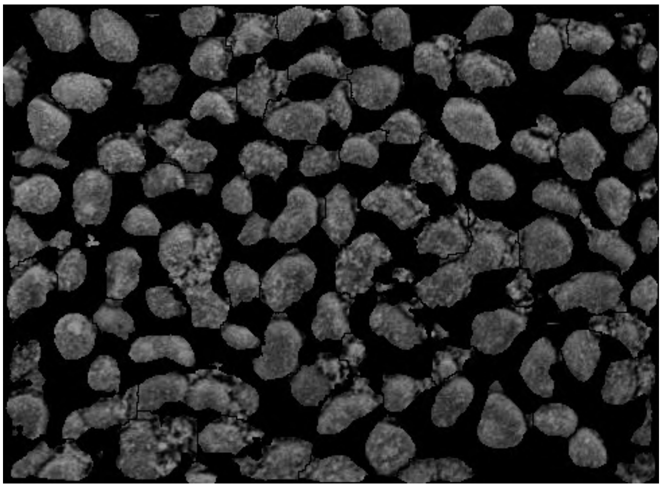

Fig. 12. Segmentation results of Mars surface image.

Table 4. The estimated parameters for the Mars surface particles

Image ID	Window Size (pixels)	Mean Diameter (μm)	Median (μm)	σ_I (μm)	SK_I	K_G	Anisotropy
Mars Particles	15	984.93	978.12	161.94	-0.029	0.968	0.339

lumping together some texture elements as a single object (see **Fig. 8**), the final result of the average diameter is impacted very slightly. This is because there are enough correct segmentation results that make the impact of incorrect ones almost negligible. In addition, this experiment demonstrates that the texture is not isotropic.

The following experiment was carried on an image of rock particles; see **Fig. 9**. The objective of this experiment is to investigate the applicability of PV on a construction material, which is of great practical value in road industry and other applications. The quality of particles delineation will be used as a metric or ground truth to judge the performance of PV. Fig. 10 shows the final results of the segmentation obtained from PV algorithm.

The segmentation results shown in **Fig. 10** suggest that PV can transform the information content of the image (here: pixels intensities) into meaningful objects (here rocks) and Table 3 presented the estimated parameters of these objects. The closeness between the mean and the median is a strong indicator that the mean diameter is a representative measure for rock distribution as captured by the image. We should also notice the robustness of the widow size of the averaging filter in terms of its relationship to the estimated mean diameter or the median. In other words, this window size does not have to be exact to get meaningful results. The anisotropy of the rocks distribution is well captured by the PV algorithm and is shown in the last column of **Table 3**.

The last experiment, reported here, was conducted on an image from Mars data (see **Fig. 11**). This is a microscopic image taken by the Mars Exploration Rover Spirit. The metric resolution of this image is 30 micrometers per pixel. That is, this image shows a dominant cluster of coarse grains (particles) distribution. The purpose of this experiment is to show the generality of PV on non-typical data set and to support the diversity argument claimed at this paper. In this experiment, the visual check of the results will be used as a metric to judge the quality of the segmentation.

The segmentation results shown in **Fig. 12** confirm the robust of the PV algorithm in terms of separating the particles from their background. The semi-identical values for the mean and the median are a strong indicator that the mean diameter can serve as a representative measure for the particles cluster distribution. As shown in the previous experiments, there is a strong anisotropy in the distribution is equal to 0.339.

4. CONCLUSIONS

This paper presents a novel and a general approach called Pixel Vernier (PV), for particle size segmentation and estimation. PV performs the particles extraction in a coarse-to-fine strategy. The markers-controlled watershed and smoothing provide a global extraction and then is refined by the minimum distance clustering algorithm. PV offers results comparable to their ground truth.

Future work should concentrate on two major issues. Firstly , embedding PV in iterative feature extraction scheme in order to estimate different ranges of particle size distributions. Secondly, upgrading PV from a supervised mode to unsupervised mode.

REFERENCES

[1] Allen, T., 1997. Particle size measurement: powder sampling and particle size measurement. Fifth edition, Vol. 1, Chapman and Hall: 525 p.

.

[2] Ibekken, H., and Schleyer, R., 1986. Photo-sieving: A method for grain-size analysis of coarse-grained unconsolidated bedding surfaces. Earth Surface Processes Landforms, vol. 11 (1): 59-77.

[3] Diepenbroek, M., Martholoma, A., and Ibekken, H., 1992. How round is round? A new approach to the topic “roundness” by Fourier grain shape analysis. Sedimentology, vol. 39 (3): 411-422

[4] Butler, J., Lane, S., and Chandler, J., H., 2001. Automated extraction of grain-size data from gravel surfaces using digital image processing. J. Hydraulic Res, vol. 39 (4): 1-11.

[5] Ghalib, A., M. and Hryciw, R., D., 1999. Soil particle size distribution by mosaic imaging and watershed analysis, J. Comput. Civil Eng. vol. 13 (2): 80-87.

[6] McEwan, I., K., Sheen, T., M., Cunningham, G., J., and Allen, A. R., 2000. Estimating the size composition of sediment surfaces through image analysis. Proc. Inst. Civil Eng., Water Maritime Eng., vol. 142 (4): 189-195.

[7] Carter, R., and Yan, Y., 2005. Measurement of particle shape using digital imaging techniques. Journal of Physics: Conference Series, 15: 177-182.

[8] Graham, D., J., Reid, I., and Rice, S., P., 2005[a]. Automated Sizing of Coarse-Grained Sediments: Image-processing procedures. Mathematical Geology, vol. 37 (1): 1-28.

[9] Tan, P., Steinbach, M., and Kumar, V., 2006. Introduction to data mining. Pearson Education: 709 p.

[10] Graham, D., J., Rice, S., P., and Reid, I., 2005[b]. A transferable method for the automated grain sizing of river gravels. Water Resources Research, vol. 41: W07020.

[11] Gonzalez, R., C., and Woods, R., E., 2002. Digital image processing. Second edition, Prentice Hall: 793 p.

[12] Shapiro, L., and Stockman, G., 2001. Computer Vision. Pearson Education: 608 p.

[13] Meyer, F., and Beucher, S., 1990. Morphological segmentation. Journal of Visual Communication and Image Representation, Vol. 1 (1): 21-46

[14] Itti, L., and Koch, C., 2001. Computational Modeling of Visual Attention, Nat. Rev. Neurosci. 2(3), pp: pages 194-203.

[15] Russ, J., C., 2002. The image processing handbook. Fourth edition, CRC Press: 732 p.

[16] Bright, D.S., and Steel, E.B., 1987. Two dimensional top hat filter for extracting spots and spheres from images. Journal of Microscopy, 146: 191-200.

[17] Otsu, N., 1979. A threshold selection method from gray-level histograms. IEEE Transaction on Systems, Man, and Cybernetics, 9: 62-66.